Supplemental Information

Solid-phase Extraction and Purification of Membrane Proteins Using a UV-modified PMMA Microfluidic Bioaffinity µSPE Device

Katrina N. Battle,[1] Joshua M. Jackson,[2] Małgorzata A. Witek [3] Mateusz L. Hupert,[3,4] Sally A. Hunsucker,[5] Paul M. Armistead,[5] and Steven A. Soper[2,3,4,6*]

[1]Department of Chemistry, Louisiana State University, 232 Choppin Hall, Baton Rouge, LA 70803-1804, USA

[2]Department of Chemistry, University of North Carolina, Campus Box 3290, Chapel Hill, NC 27599-3290, USA

[3]Department of Biomedical Engineering, University of North Carolina,152 MacNider Hall Campus Box 7575 Chapel Hill, NC 27599-7575, USA

[4] BioFluidica, LLC, c/o Carolina Kick-Start, 321 Bondurant Hall, Chapel Hill, NC, 27599

[5]Lineberger Comprehensive Cancer Center, University of North Carolina School of Medicine, Chapel Hill, NC, USA

[6]School of Nano-Bioscience and Chemical Engineering, Ulsan National Institute of Science and Technology, Ulsan, Republic of Korea

*Corresponding author
Phone: (919) 843-5575
Email: ssoper@unc.edu

Experimental Section

Membrane protein extraction. Membrane proteins were extracted using a Mem-PER™ Plus Membrane Protein Extraction Reagent kit following the manufacturer's protocol. Approximately 5 x 10^6 MCF-7 cells were harvested from the culture dish by incubating with TrypLE Express cell dissociation reagents for 5-10 min and then centrifuged. The pellet was washed with 3 mL of the kit's cell wash solution and the resultant solution centrifuged. The supernatant was removed and discarded, and the cell pellet was resuspended in 1.5 mL of a cell wash solution, transferred to a centrifuge tube, and centrifuged with the supernatant discarded. 750 µL of permeabilization buffer was added to the cell pellet and briefly vortexed to obtain a homogeneous solution. The pellet was then incubated at 4ºC for 10 min with constant mixing. After incubation, the cells were centrifuged at 16,000× g for 15 min with the supernatant discarded, which contained the cytosolic proteins. 500 µL of a solubilization buffer was added to the remaining cell pellet and the cells were resuspended and incubated at 4ºC for 30 min with constant mixing. Lastly, centrifugation was done at 16,000x g for 15 min and 4ºC. The remaining supernatant contained the solubilized membrane and membrane-associated proteins.

Biotinylation of MCF-7 cells. In order to determine if MCF-7 cells were indeed biotinylated, we used FITC-conjugated avidin to visualize the cells that had been reacted with sulfo-NHS-SS-biotin. After biotinylation and removal of excess reagent, a 10 µL aliquot of a 100X diluted solution of FITC-avidin (1X in PBS) was added to 1 mL of the biotinylated cells (PBS) and incubated at room temperature (covered in aluminum foil) for 30 min. After incubation, the cells were washed thoroughly to remove excess FITC-avidin from the solution. The cells were then visualized using a Carl Zeiss Axiovert 200M inverted microscope coupled to a 75 W XBO lamp. The images of these cells are shown in Figure S1. As can be seen, the MCF-7 cells were fluorescent indicative of successful biotinylation.

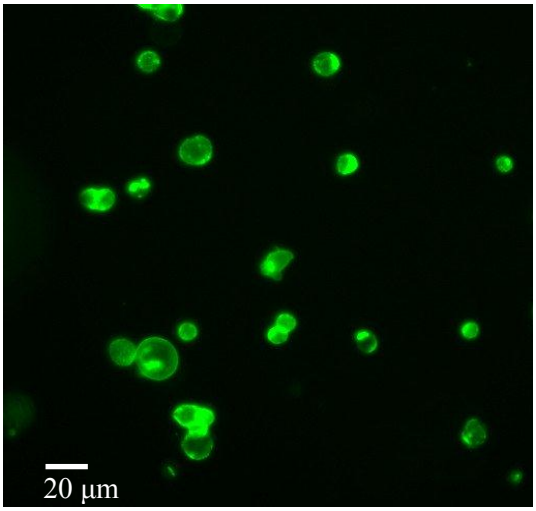

Figure S1. Fluorescence image taken at 488/520 nm excitation/emission (20x, 200 ms exposure time) of biotinylated MCF-7 cells that had been incubated with FITC-conjugated avidin.

Experimental workflow. In addition to Scheme 1, Table S2 summarizes the experimental workflow for preparation of the µSPE device and isolation, purification, visualization, and quantification of the biotinylated membrane proteins as well as their removal from the extraction bed.

Table S2. Summary of workflow for the µSPE of biotinylated membrane proteins.

Assay Step	Purpose	Method
Device activation	To generate carboxylic acid functionalities for NeutrAvidin immobilization	Irradiate PMMA micropillars (254 nm, 22 mW/cm^2) for 15 min
NeutrAvidin immobilization	EDC/NHS activates carboxylic acids on micropillar surfaces for NeutrAvidin immobilization	EDC/NHS activation (30 min at room temperature) and infusion of NeutrAvidin and incubation overnight at 4°C
Membrane protein extraction	Isolate biotinylated proteins via NeutrAvidin immobilized in µSPE bed	Infuse cell lysate at constant flow rate
Purification	Remove cytosolic contaminants	High salt (1 M KCl), high pH (11.5) wash
Visualization	Bind FITC-avidin to unbound biotins on the membrane proteins to visualize bound membrane proteins	Infuse FITC-avidin solution; PBS wash to remove nonspecific FITC-avidin; visualize via fluorescence microscopy
Elution of membrane proteins	Reduce disulfide bond of biotin moiety and quantify release of protein	Incubate with 300 mM DTT; analyze effluent (biotinylated membrane proteins and FITC-avidin) with fluorometer

Results and Discussion

Computation fluid dynamics (CFD) analysis of velocity fields, diffuse protein transport, and protein extraction in different µSPE bed configurations. For the CFD simulations, three model geometries composed of staggered rows of micropillars were tested (see Figure S2): (I) Circular pillars with diameters of 100 µm and pillar-to-pillar spacing of 50 µm; (II) diamond-shaped pillars with a side length of 20 µm (fileted by 5 µm to reflect the fabrication limits of micro-milling) and a pillar-to-pillar spacing of 20 µm; and (III) circular pillars with radii of 20 µm and a pillar-to-pillar spacing of 20 µm. In all geometries, the number of pillars was restricted to only a few staggered rows (relative to the hundreds occupying a single µSPE bed) to ensure numerical tractability of the simulations.

Using these geometries, CFD simulations of steady-state laminar flow through the µSPE beds were evaluated using COMSOL Multiphysics to provide the velocity fields shown in Figure S2. For comparison, µSPE beds were designed within COMSOL to have the same fluidic inlet with the fluid

(modeled with the properties of water) entering the beds assigned a linear velocity of 0.83 mm s^{-1} to reflect a volumetric flow rate of 1 µL min^{-1}.

Throughout each bed, the flow velocity (and thereby reagent flux) was uniform, indicating that protein solutes uniformly infused through the µSPE bed and were distributed across the entirety of the µSPE's surface area. However, these results do not reflect the effects of diffusion (*i.e.*, diffusion of protein into adjacent flow streams that may be in proximity to the extraction surface) or how device geometry, such as micropillar shape or pillar-to-pillar spacing, encourages diffusion into these flow streams. For this, we conducted diffusion calculations in the subsequent section using average protein velocities through the µSPE bed geometries that were extracted from the velocity fields in Figure S2.

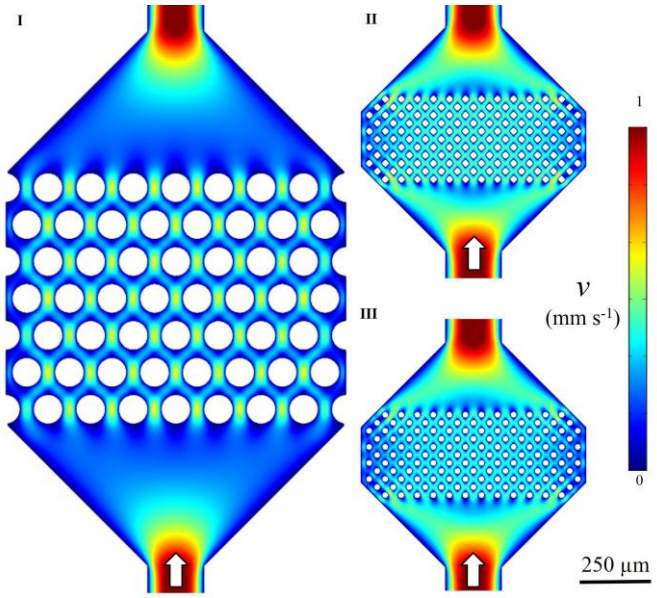

Figure S2. Steady-state velocity profiles of µSPE bed geometries I-III. Flow fields are scaled in both size and magnitude. The solid-white arrows indicate the direction of flow.

Diffusion model for approximating the effects of micropillar geometry on effective bed length and protein extraction. Only biotinylated proteins within a few nanometers of the µSPE bed's surface may be extracted by the surface-confined NeutrAvidin molecules. Initial protein in these active flow lines are likely to be rapidly depleted; the protein molecules not resident within these flow lines must necessarily diffuse to the µSPE bed's surface for extraction to take place, a phenomenon that occurs over a time proportional to the µSPE bed's entire length (L = 24 mm) and the protein's average velocity (v).

In general, the axial position of a protein in a fluidic channel (x) may be described as a Gaussian probability packet that spreads in time according to its diffusion coefficient (D) and an analytic solution to Fick's second law:

$$P(x,t) = \frac{1}{\sqrt{2\pi\sigma^2}} e^{\left(-\frac{x^2}{2\sigma^2}\right)} \quad (1)$$

where *P(x,t)* is the probability that a protein occupies axial position *x* at time *t* according to a Gaussian packet with standard deviation $\sigma = \sqrt{2Dt} = \sqrt{2DL/v}$.

If we consider a worst case scenario, where a protein has the initial position exactly centered between two pillars ($x = 0$) that have a pillar-to-pillar spacing of W_s (boundary conditions of $\pm W_s/2$), the probability that a protein has diffused to and interacted with the pillars (P_i) during its transit through the µSPE bed is given by integration of the following equation:

$$P_i(t = C \cdot L/\bar{v}) = 2\int_{|x|=W_s/2}^{\infty} P(x, t = C \cdot L/\bar{v})dx \quad (2)$$

A simple method of performing this integration uses z-scores associated with the Gaussian packet, where $z(x) = x/\sigma$ and $P_{z(x)}$ is the normalized area of the Gaussian packet from $-\infty$ to $z(x)$. Thus, Eq. (2) can be simplified to:

$$P_i(t = C \cdot L/\bar{v}) = 1 - \left[P_{z\left(x=\frac{W}{2}\right)} - P_{z\left(x=\frac{-W}{2}\right)}\right] \quad (3)$$

Eq. (3) can be solved with a standard Excel spreadsheet by calculating $\sigma = \sqrt{2D \cdot L/\bar{v}}$ and solving for $z\left(x = \pm\frac{W}{2}\right)$ and P_z using the NORMSDIST function. Operations given by Eqs. (2) and (3) are illustrated in Figure S3 for convenience.

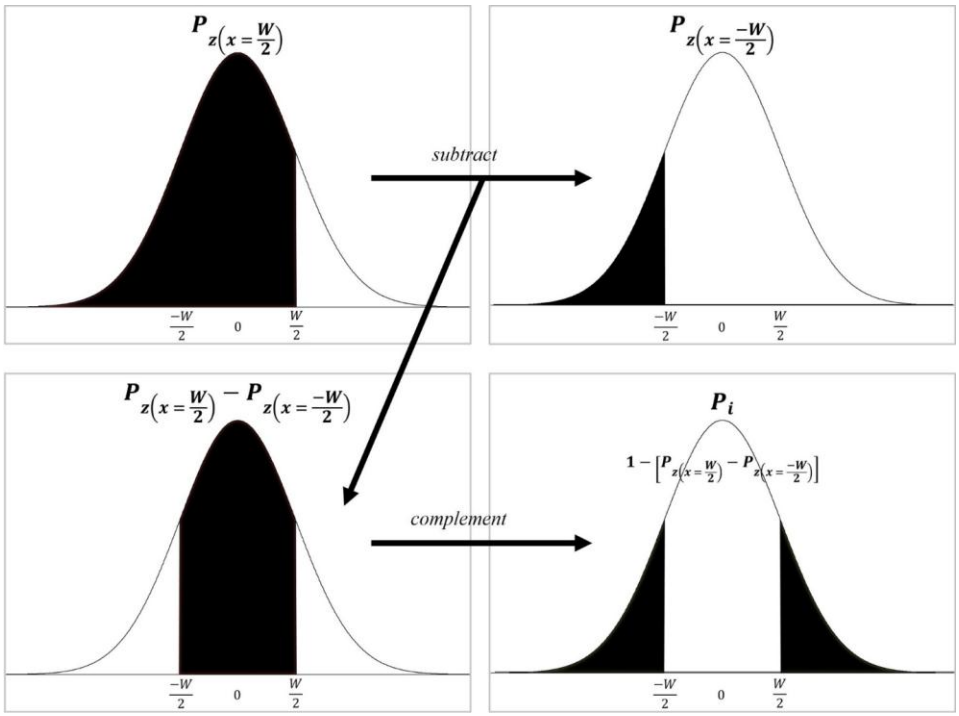

Figure S3. Schematic for calculating the probability of a protein extracted by the µSPE beds' micropillars (P_i) from the time-dependent Gaussian probability packets and the analytical solution to Fick's 2nd law.

In Figure 5, we show the solutions for geometries I-III. Here, we used the average velocities through the µSPE beds for geometries I-III that were obtained via the simulation results shown in Figure S2 and scaled these velocities proportionally for higher and lower flow rates.

It should be noted that a protein does not travel linearly through the bed; instead it will circumnavigate micropillars and travel an effective length, $\mathrm{L_{eff}} = \mathrm{C} \times \mathrm{L}$, where C is a geometric correction factor intimately tied to the pillar shape. Thus, the fact that micropillars create obstacles, which fluid must flow around, increases the time for protein diffusion to occur as well as the probability of extraction. For circular pillars, the protein will travel about a half circumference yielding, $\mathrm{C} = \pi/2 \approx 1.57$; for diamond pillars, the protein travels about a triangle yielding, $\mathrm{C} = \sqrt{2} \approx 1.41$. These assignments can be shown to be independent of the pillar size, which are geometrically illustrated in Figure 5 and can be represented by simply substituting L_{eff} for L in Eqs. (2) and (3). Consequently, the effective path length of proteins traveling through µSPE beds with circular pillars is slightly longer than that of µSPE beds with diamond pillars due to the larger perimeter of (and path length of fluid around) circular micropillars permitting increased time for diffusion to occur and improved probability that proteins interact with the pillars and thus are recovered.

We must note that this model is a simplification of actual diffusion effects in the µSPE beds. Average velocities extracted from the velocity fields in Figure S2 were applied to protein diffusion irrespective of the protein's position in time. Realistically, as the protein diffuses away from the central $x = 0$ position, its velocity decreases according to Poiseuille flow, and the time scale available for diffusion would increase. Thus, there is some error in the absolute time scales over which diffusion occurs, and the results presented herein represent an underestimation of device efficiency. To correct this assumption, the average velocity term $\bar{v}$ in Eqs. (2) and (3) would be replaced with a position dependent velocity term, $v(x)$, but this would require a formulation within COMSOL itself because flow in the µSPE bed is not equivalent to a straight channel as can be seen in Figure S2; there is a large discrepancy between flow velocity between micropillars and in the areas between rows of micropillars.

This model must be treated as a simplification of diffusion effects and the efficiency of protein extraction in the µSPE beds, and one should only take meaning in the relative impact of volumetric flow rate and micropillar shape and spacing on protein extraction efficiency rather than absolute efficiency itself. Thus, the results in Figure 5 indicate that future µSPE bed designs should incorporate circular micropillars with reduced pillar-to-pillar spacing (discussed further in the main text).